

Local and Remote Responses of Atmospheric and Oceanic Heat Transports to Climate Forcing: Compensation versus Collaboration

ZHENGYU LIU

Atmospheric Sciences Program, Department of Geography, The Ohio State University, Columbus, Ohio

CHENGFEI HE

*College of Atmospheric Sciences, Nanjing University of Information Science and Technology, Nanjing, China, and
Atmospheric Sciences Program, Department of Geography, The Ohio State University, Columbus, Ohio*

FEIYU LU

*Department of Atmospheric and Oceanic Sciences, and Center for Climatic Research, University of Wisconsin–Madison,
Madison, Wisconsin, and NOAA/Geophysical Fluid Dynamics Laboratory, Princeton, New Jersey*

(Manuscript received 12 October 2017, in final form 18 May 2018)

ABSTRACT


We present a theoretical study on local and remote responses of atmosphere and ocean meridional heat transports (AHT and OHT, respectively) to climate forcing in a coupled energy balance model. We show that, in general, a surface heat flux forces opposite AHT and OHT responses in the so-called compensation response, while a net heat flux into the coupled system forces AHT and OHT responses of the same direction in the so-called collaboration response. Furthermore, unless the oceanic thermohaline circulation is significantly changed, a remote climate response far away from the forcing region tends to be dominated by the collaboration response, because of the effective propagation of a coupled ocean–atmosphere energy transport mode of collaboration structure. The relevance of our theory to previous CGCM experiments is also discussed. Our theoretical result provides a guideline for understanding of the response of heat transports and the associated climate changes.

1. Introduction

The coupled ocean–atmosphere system transports ~ 5 PW (1 PW = 10^{15} W) of energy poleward in the atmosphere and ocean combined (Stone 1978a; Trenberth and Caron 2001; Wunsch 2005). Despite their critical roles in maintaining our climate, the responses of atmospheric heat transport (AHT) and oceanic heat transport (OHT) to climate forcing have remained poorly understood. Many previous studies in coupled general circulation models (CGCMs) have shown a robust compensation of heat transport responses between AHT and OHT anomalies (e.g., Broccoli et al. 2006; Held and Soden 2006; Kang et al. 2008; Zelinka and

Hartmann 2012; Rose and Ferreira 2013; Marshall et al. 2014; Farneti and Vallis 2013) in the so-called Bjerknes compensation response (Bjerknes 1964), or called simply the “compensation” response here. However, in recent CGCM experiments to high-latitude climate forcing, AHT and OHT are found to respond in collaboration with the response in the same direction (Deser et al. 2015; Hawcroft et al. 2016; Haywood et al. 2016; Kay et al. 2016; Green and Marshall 2017) in what we call here a “collaboration” response. These seemingly contradictory studies raise a fundamental question. What is the mechanism determining the responses of the meridional heat transports in the atmosphere and ocean?

To understand the mechanism of the Bjerknes response, conceptual models like energy balance models (EBM) or box models have been used in previous works [see reviews in Liu et al. (2016) and Yang et al. (2016)]. Most recently, we have studied the mechanism for

 Denotes content that is immediately available upon publication as open access.

Corresponding author: Zhengyu Liu, liu.7022@osu.edu

DOI: 10.1175/JCLI-D-17-0675.1

© 2018 American Meteorological Society. For information regarding reuse of this content and general copyright information, consult the [AMS Copyright Policy](https://www.ametsoc.org/PUBSReuseLicenses) (www.ametsoc.org/PUBSReuseLicenses).

Bjerknes compensation in an EBM (Liu et al. 2016) and a box model (Yang et al. 2016) to a perturbation OHT systematically. Our studies suggest that, in response to a change of OHT, AHT always changes in the opposite direction, or in the compensation response, as long as the overall climate feedback is negative through the top of the atmosphere (TOA) so that the climate system is stable. Furthermore, our studies suggest that, in the case of local positive feedback, the AHT response magnitude can exceed that of the perturbation OHT forcing in a so-called overcompensation response. These previous works nevertheless have left important questions on heat transport responses unanswered. Here, we are concerned with two questions.

- Question 1: What is the coupled response of AHT and OHT to a general climate forcing, such as a radiative forcing?
- Question 2: What is the remote response of the coupled heat transport to a local perturbation forcing?

Liu et al. (2016) and Yang et al. (2016) cannot address question 1 because they address only the response of the AHT to a perturbation OHT, which is thought to be induced by either a collapse of the Atlantic meridional overturning circulation (AMOC) in the fully coupled model (or the real world) or a prescribed OHT anomaly in an idealized coupled model with the atmosphere and a slab ocean. Liu et al. (2016) and Yang et al. (2016) cannot address question 2, because their perturbation forcing (in OHT) is either prescribed over the globe or caused by the collapse of the AMOC, whose deep ocean current transports anomalous heat transport efficiently across the globe.

Here, we extend Liu et al. (2016) and Yang et al. (2016) to address these two questions by using a coupled EBM with active OHT. Our study predicts a compensation response to a surface heat flux forcing but a collaboration response to a net heat flux into the coupled system. Furthermore, the remote response tends to be dominated by the collaboration response because of the effective propagation of an energy transport mode, unless the oceanic thermohaline circulation is perturbed significantly. The paper is arranged as follows. Section 2 presents our model. The local response and remote responses of AHT and OHT are discussed in sections 3 and 4, respectively. In section 5 we discuss the heat transport response to global warming forcing. A summary and further discussion are given in section 6.

2. The coupled model

To illustrate the physical mechanism more clearly, we use the zonal mean EBM (North 1975) adapted to the coupled atmosphere–ocean system (Farneti and Vallis

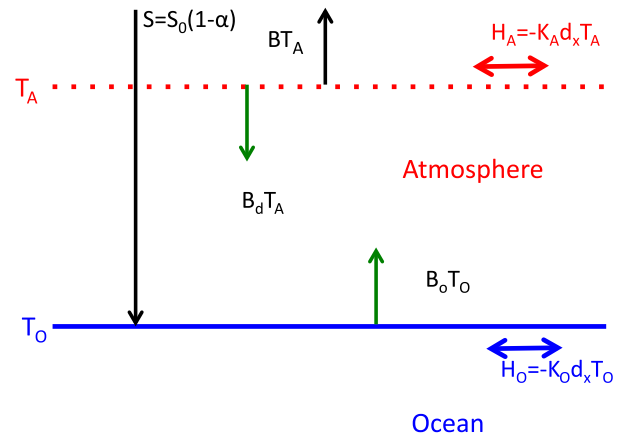


FIG. 1. Schematic figure of the coupled EBM in Eqs. (1a) and (1b). Green arrows represent heat fluxes across the air–sea interface, while black arrows indicate net heat fluxes into the coupled system. For simplicity, an upward IR through TOA is not included here.

2013; Shell and Somerville 2005; Rose and Marshall 2009) as a coupled EBM (Fig. 1),

$$0 = F_T - F_S - d_x H_A \quad \text{and} \quad (1a)$$

$$0 = S + F_S - d_x H_O, \quad (1b)$$

with d_x representing the derivative in latitudinal distance x . Here, S is the solar radiation at the surface; the infrared radiation (IR) at TOA is

$$F_T = -BT_A. \quad (1c)$$

The net surface heat flux is the sum of the upward heat flux from the ocean $-B_O T_O$ and the downward heat flux from the atmosphere $B_d T_A$ as follows:

$$F_S = -B_O T_O + B_d T_A, \quad (1d)$$

with T_A and T_O representing the temperatures in the mid-troposphere and ocean surface, respectively. Typical values for the feedback parameters are $B = 2.83 \text{ W m}^{-2} \text{ K}^{-1}$, $B_d = 11.3 \text{ W m}^{-2} \text{ K}^{-1}$, and $B_O = 10.4 \text{ W m}^{-2} \text{ K}^{-1}$ (e.g., Farneti and Vallis 2013). Note that for realistic scenarios, the values of the surface downward and upward feedback parameters B_d and B_O , respectively, are significantly larger than the TOA radiative parameter B , because B_d and B_O include not only IR radiative feedbacks but also the strong air–sea negative feedback through the turbulent heat flux. This turns out to be important for understanding the remote response of heat transports, as will be discussed in section 4. For convenience, however, sometimes we still refer to B_d and B_O as IR flux feedback parameters. In the equations here, global means have been removed from these

energy fluxes so we can focus on the spatial gradient and the associated heat transport. The heat transport is parameterized as the diffusion of atmospheric temperature for AHT (North 1975; Stone 1978b),

$$H_A = -K_A d_x T_A, \quad (1e)$$

and as the diffusion of sea surface temperature for OHT (Farneti and Vallis 2013; North 1975; Longworth et al. 2005; Rose and Marshall 2009),

$$H_O = -K_O d_x T_O. \quad (1f)$$

Typical diffusivities are $K_A = 8 \times 10^{13} \text{ kg}^2 \text{ s}^{-1}$ and $K_O = 2 \times 10^{13} \text{ kg}^2 \text{ s}^{-1}$. Some simplifications have been adopted in the atmospheric model. All the feedback coefficients are assumed to be spatially uniform. A small outgoing TOA IR flux emitted from the surface is also neglected (but is included later in section 5). The atmospheric energy could be generalized to include the moisture effect explicitly as the moisture static energy, as in Liu et al. (2016). The ocean model is also highly simplified. The OHT parameterization, albeit crude, may represent some coupled features of the OHT associated with the upper-ocean wind-driven circulation (Vallis and Farneti 2009). With all the parameterizations in Eqs. (1c)–(1f), the coupled system [Eqs. (1a) and (1b)] can be written as

$$0 = -(B + B_d)T_A + B_O T_O + K_A d_{xx} T_A \quad \text{and} \quad (2a)$$

$$0 = S - B_O T_O + B_d T_A + K_O d_{xx} T_O. \quad (2b)$$

It should be pointed out that it is this active OHT here that generalizes the coupled EBM beyond Liu et al. (2016), where the atmospheric EBM is coupled with a slab ocean and therefore can be used only to study the response of AHT to a perturbation OHT. Here, instead, the coupled model can be used to study the active responses of both AHT and OHT to a general climate forcing.

3. Forced response

In this section we address question 1: What are the responses of both AHT and OHT to a general climate forcing on a coupled system? The responses to a perturbation climate forcing can be derived from Eqs. (2a) and (2b) conveniently in the Cartesian coordinate with the no-flux boundary condition $d_x T_A = d_x T_O = 0$ over the domain $[-\pi/2, \pi/2]$ using the eigenfunction of the Laplace operator d_{xx} : $\sin(nx)$, $n = 1, 3, 5, \dots$ for anti-symmetric responses. Symmetric responses can be derived similarly using eigenfunctions $\cos(nx)$, $n = 2, 4, 6, \dots$. All results can also be obtained similarly in the spherical

coordinate, as in Liu et al. (2016). Given a climatology solar forcing $S = S_n \sin(nx)$, the climatology temperature can be derived as follows:

$$T_A = T_{A_n} \sin(nx), \quad T_O = T_{O_n} \sin(nx),$$

where the temperature amplitudes are

$$T_{A_n} = B_O S_n / G, \quad T_{O_n} = (B + B_d + K_A n^2) S_n / G,$$

with

$$G = (B_O + K_O n^2)(B + K_A n^2) + K_O n^2 B_d.$$

The corresponding heat transports can be calculated using Eqs. (1e) and (1f) as follows:

$$H_A = -h_A \cos(nx), \quad H_O = -h_O \cos(nx),$$

with the amplitudes as

$$h_A = n K_A T_{A_n}, \quad h_O = n K_O T_{O_n}.$$

Now, we impose a small perturbation forcing δf , where f can represent the forcing parameter for OHT K_O , AHT K_A , atmospheric downward flux B_d or upward IR B , oceanic upward flux B_O , or solar radiation S . In the limit of weak forcing, the ratio of the heat transport responses in AHT δh_A and OHT δh_O , or the so-called Bjerknes compensation (BJC) ratio, can be calculated as the ratio of the derivatives,

$$C_f = \delta h_A / \delta h_O = \partial_f h_A / \partial_f h_O.$$

This leads to the BJC ratio for each individual forcing as follows:

$$C_{K_O} = C_{B_O} = C_{B_d} = -\frac{1}{1 + B/(K_A n^2)}, \quad (3a)$$

$$C_{K_A} = -1 - \frac{B(B_O + K_O n^2)}{B_d K_O n^2}, \quad (3b)$$

$$C_S = \frac{K_A B_O}{K_O (B + B_d + K_A n^2)}, \quad \text{and} \quad (3c)$$

$$C_B = \frac{K_A (B_O + K_O n^2)}{K_O B_d}. \quad (3d)$$

To understand these responses, we start with the response to OHT, which always exhibits a compensation response ($C_{K_O} < 0$). Physically, a perturbation OHT leads to a surface energy flux into the atmosphere in the oceanic downstream region due to the OHT convergence; this energy flux is partly damped into the space by the negative TOA climate feedback ($-B < 0$), leaving the rest of heat flux to be transported back in the

opposite direction in AHT. The BJC response here can be seen in the example in Fig. 2. The perturbation forcing is now caused by a reduction of K_O uniformly over the globe (Fig. 2e). The forced responses in temperatures, heat transports, the BJC ratio, and the energy budget are then shown in Figs. 2a–d, respectively. It is seen that the reduction of K_O leads to a reduction in the northward OHT (blue, Fig. 2b), which causes an anomalous OHT divergence (convergence) and in turn surface heat flux cooling (warming) to the atmosphere (red solid, Fig. 2d) and, eventually, a dipole temperature response of northern (southern) cooling (warming) (Fig. 2a). This surface cooling (warming) is eventually balanced by a combined warming (cooling) from an AHT convergence (divergence) (red dotted, Fig. 2d) and a reduction (enhancement) of TOA IR cooling in the north (south) (red dashed, Fig. 2d). The northward AHT anomaly (Fig. 2b) is opposite of the OHT anomaly, corresponding to a compensation response everywhere across the globe (Fig. 2c). The mechanism of the compensation response is qualitatively the same as discussed in Liu et al. (2016) and Yang et al. (2016) because, in this case, OHT is changed first (by the reduction of K_O) and therefore is essentially a case of an AHT response to a perturbation OHT forcing. Here, it is interesting that the BJC ratio [Eq. (3a)] is exactly the same form as in the EMB with a slab ocean under a prescribed OHT forcing (Liu et al. 2016) or a box model with active thermohaline dynamics (Yang et al. 2016). This suggests the robustness of the BJC ratio estimation here. The compensation response is also consistent qualitatively with those where atmosphere general circulation models are coupled with a slab ocean model (Kang et al. 2008), confirming the compensation response to an OHT forcing in general. As pointed out earlier, the compensation response in Fig. 2 may be thought of as an analogy of a reduction of oceanic thermohaline transport through an ocean tunnel induced by, say, a high-latitude freshwater flux in the Southern Hemisphere (SH). This is illustrated schematically in Fig. 3a. Indeed, at equilibrium, the OHT associated with the thermohaline may be represented using a diffusive heat flux, with the diffusivity K_O proportional to the thermohaline transport (Stommel 1961). This BJC ratio in Eq. (3a) is also the same as that derived in a box model with active thermohaline dynamics (Yang et al. 2016).

Now, we study the responses to general climate forcing. The general responses in Eqs. (3a)–(3d) show a clear pattern of heat transport responses: a compensation response is forced by a surface heat flux forcing, related to either K_O , K_A , B_d , or B_o , as shown in Eqs. (3a) and (3b); and a collaboration response is generated by a TOA net heat flux forcing, related to either S or B , as

THC-Compensation Response to K_o

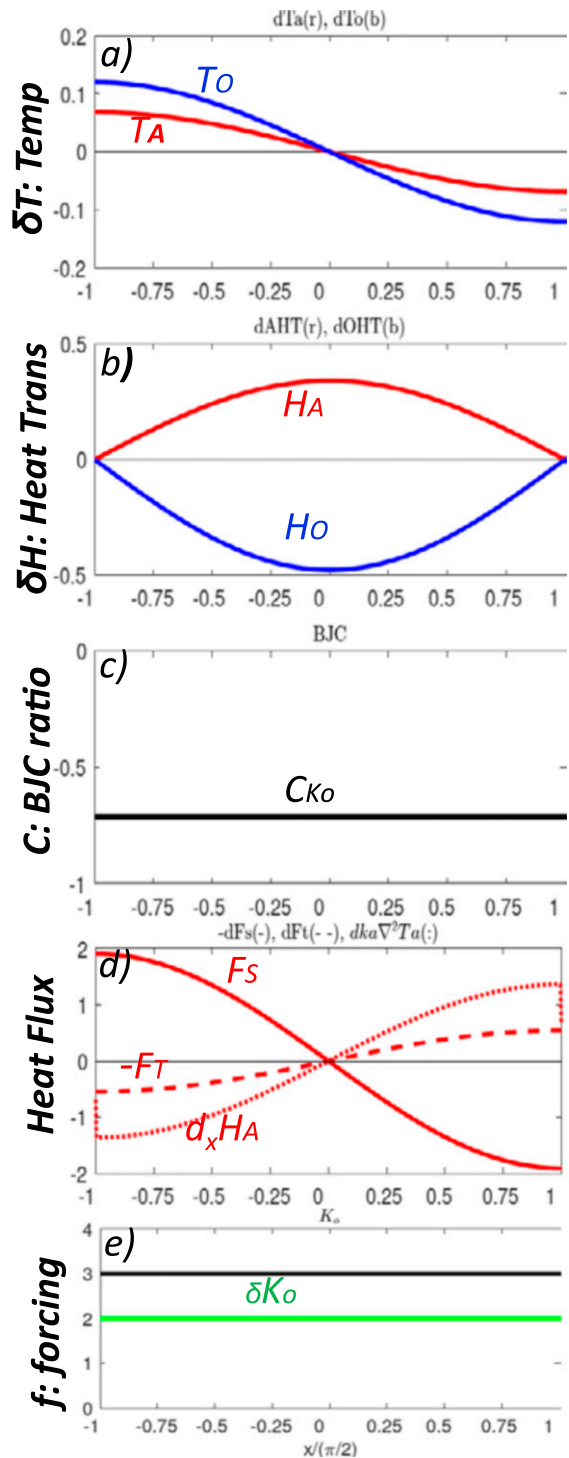


FIG. 2. Heat transport responses forced by a decrease in ocean diffusivity K_O over the globe. (a) Temperature responses for the atmosphere (solid red) and ocean (solid blue); (b) responses for AHT (solid red) and OHT (solid blue); (c) BJC ratio (solid black); (d) atmospheric energy budget: upward surface heat flux F_S (solid), downward TOA IR flux $-F_T$ (dashed), and AHT convergence (dotted); (e) forcing parameters for the control (black) and perturbation (green) experiments.

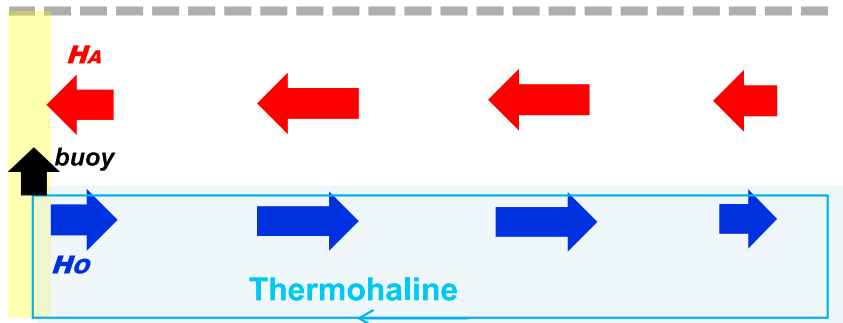
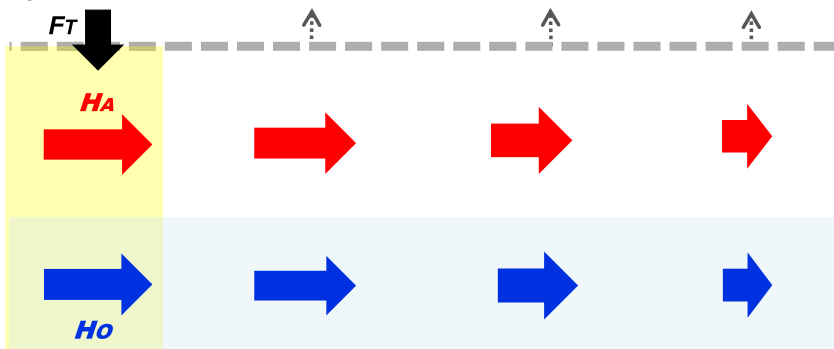
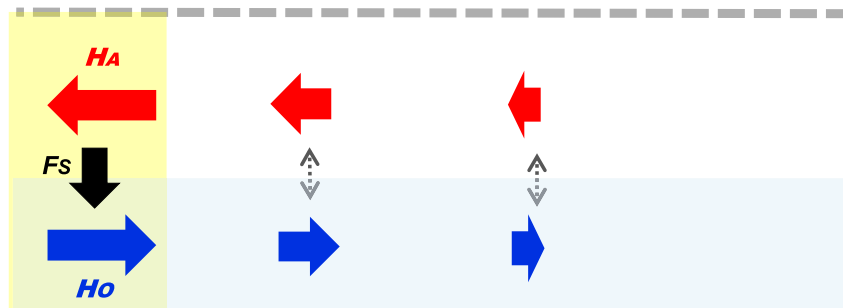
Forced Response**Free Mode
“Propagation”****a) THC-Compensation Mode****b) Coupled Collaboration Mode****c) Coupled Compensation Mode**

FIG. 3. Schematic figures showing the heat transport response to different forcings. (a) Global compensation response forced by a perturbation thermohaline forcing. (b) Regional collaboration response forced by the TOA heat flux F_T (shading region) and the subsequent propagation in the collaboration mode. (c) Regional compensation response to surface heat flux F_S and the damped response in the far field following the compensation mode.

shown in Eqs. (3c) and (3d). This can be understood physically as follows. A surface air–sea exchange flux always exerts the opposite heat flux forcing to the atmosphere and ocean, as seen in Eqs. (1a) and (1b) or Eqs. (2a) and (2b), and therefore tends to drive the

opposite AHT and OHT responses. This surface flux can be accomplished directly by radiative and turbulent heat fluxes at the surface in F_S (related to either B_d or B_o), or indirectly by the OHT divergence $d_x H_o$ (related to K_o) or AHT divergence $d_x H_A$ (related to K_A). In retrospect,

to the authors, this qualitative understanding of the different heat transport compensation responses to TOA and surface forcing is obvious. This general idea might have been realized by some researchers in the past. However, we are not aware of any publication clearly stating this point. Here, we prove these opposite compensation responses unambiguously in EBM.

Our analytical solution further enables us to derive the BJC ratio under each forcing quantitatively. It is interesting that the BJC ratios are exactly the same for all three surface forcings— C_{K_O} , C_{B_d} , and C_{B_O} —as shown in Eq. (3a). This is further evidence of the robustness of the compensation response to a general surface forcing. In contrast, a net heat flux at TOA, such as the TOA IR [$C_B > 0$; Eq. (3d)] and solar radiation [$C_S > 0$; Eq. (3c)], represents a net energy import into the coupled system that can be transported away by AHT and OHT collaboratively in the same direction. A natural example of collaboration response is the observed climatology in which solar radiation forces both the AHT and OHT poleward (Trenberth and Caron 2001; Wunsch 2005). It should be noted that the OHT forcing can change the AHT only because its convergence induces a surface flux forcing; therefore, it is best thought of as an indirect surface flux forcing (in the case of equilibrium response here). Indeed, in the ocean [Eq. (1b)], if the perturbation forcing is due to OHT only, we have $\delta(S) = 0$ and therefore $\delta F_S = \delta(d_x H_O)$. The equivalence between the perturbation OHT forcing and perturbation surface forcing offers an explanation for the robustness of the compensation response to a perturbation OHT associated with a changing thermohaline (e.g., Zhang and Delworth 2005; Vellinga and Wu 2008): the convergence of OHT is equivalent to a surface flux forcing and therefore will force a robust compensation response.

One may note a difference in the magnitude of the BJC ratios between the responses to K_O , B_d , or B_O in Eq. (3a) and the response to K_A in Eq. (3b): Although all the responses are compensation responses ($C < 0$), the response to K_O , B_d , or B_O has a smaller AHT magnitude relative to OHT—that is, $|C_{K_O}| = |C_{B_d}| = |C_{B_O}| < 1$ —which has been called an undercompensation response (Liu et al. 2016; Yang et al. 2016). In contrast, the coupled response to K_A has a greater AHT magnitude than OHT—that is, $|C_{K_A}| > 1$ —which has been called an overcompensation response (Liu et al. 2016; Yang et al. 2016). Physically, the compensation response to AHT forcing ($C_{K_A} < 0$) can be understood similarly to that for OHT. Since the coupled system exhibits negative feedback at the TOA everywhere ($-B < 0$), in response to an OHT forcing, the atmospheric temperature response is damped by the TOA negative feedback, leaving less AHT to return back, that is, an undercompensation to OHT forcing

($|C_{K_O}| = |\delta h_A / \delta h_O| < 1$) (Liu et al. 2016; Yang et al. 2016). Similarly, an initial AHT perturbation forcing will force the atmospheric temperature anomaly to be damped by the negative feedback, leaving less energy to be transported back by the OHT, which is equivalent to an undercompensation response to the AHT forcing ($1/|C_{K_A}| = |\delta h_O / \delta h_A| < 1$). Here, the lack of positive feedback is important. Otherwise, with regional positive feedback [$-B(x) > 0$], the response could be locally overcompensated ($|C_{K_O}| > 1$ to OHT (Liu et al. 2016; Yang et al. 2016) and, similarly, locally undercompensated ($|C_{K_A}| < 1$ to AHT).

In summary, the compensation response in Eqs. (3a)–(3d) gives a clear heat transport response for each individual forcing, with surface flux forcing compensation and TOA net flux forcing collaboration. It should be noted, however, that the response is usually not so clean in more realistic scenarios. A realistic forcing, such as that for global warming, dust loading, or cloud change, usually perturbs both the surface and TOA fluxes. Therefore, the ultimate heat transport response would depend on the competition between surface and TOA forcing. One example of such mixed forcing is the global warming case and will be discussed later in section 5.

4. Remote response

Now, we turn to question 2: What is the remote response of heat transports to a localized forcing? Physically, the remote response is determined by the “propagation” of the coupled energy transport modes. For the equilibrium response here, these energy modes are all stationary modes, and therefore a temporally damped mode becomes a spatially damped mode. Different modes exhibit different spatial damping scales in their propagation away from the forcing region. These free modes can be derived by setting the forcing $S = 0$ in the linear Eqs. (2a) and (2b). In the case of a constant coefficient here, these modes can be derived analytically. We assume that temperatures are in the modal structures as

$$T_A(x) = q_A e^{-\lambda x}, \quad T_O(x) = q_O e^{-\lambda x},$$

where λ is the spatial damping rate. For simplicity, we can assume λ to be positive for a mode of increasing x .¹ Substituting T_A and T_O into Eqs. (2a) and (2b), we have the eigenequations

$$K_A(\mu - \mu_A)q_A + \mu_O K_O q_O = 0 \quad \text{and} \\ b_d K_A q_A + (\mu - \mu_O)K_O q_O = 0,$$

¹For the full solution that strictly satisfies no-flux boundary condition at both poles, as in Figs. 4 and 5, both modes of positive and negative λ are required.

where $\mu = \lambda^2$ is the damping rate square, and

$$\mu_A = b + b_d \equiv (B + B_d)/K_A,$$

and

$$\mu_O = b_O \equiv B_O/K_O$$

are the damping rate squares for the uncoupled atmospheric and oceanic modes, respectively, as will be seen soon. The eigenvalue equation can therefore be derived as follows:

$$(\mu - \mu_A)(\mu - \mu_O) - b_d b_O = 0, \quad (4)$$

and the eigenvalue is then

$$\mu_{\pm} = \frac{\mu_A + \mu_O \pm \sqrt{\Delta}}{2},$$

where $\Delta = (\mu_A + \mu_O)^2 - 4b_d b_O$.

In the absence of ocean–atmosphere coupling, $b_d b_O = 0$, Eq. (4) shows that the two modes are uncoupled such that one mode is the pure atmospheric mode with $\mu = \mu_A$, and the other mode is the pure oceanic mode with $\mu = \mu_O$, each decaying at its own rate. In general, $\Delta > 0$, because $b_d, b_O, b > 0$, and it is straightforward to show that $\Delta \equiv b_d^2 + 2b_d(b + b_O) + (b - b_O)^2$. Now, the coupled system has two coupled modes. One mode (μ_+) has a stronger damping rate than both the atmosphere and ocean,

$$\mu_{\text{COMP}} \equiv \mu_+ > \max(\mu_A, \mu_O); \quad (5a)$$

its eigenfunction exhibits a compensation structure as calculated from its BJC ratio

$$C = \frac{K_A d_x T_A}{K_O d_x T_O} = \frac{K_A q_A}{K_O q_O},$$

as

$$C_{\text{COMP}} \equiv C_+ = \frac{b_O}{\mu_A - \mu_+} = \frac{\mu_O - \mu_+}{b_d} < 0. \quad (5b)$$

Therefore, this mode will be called the coupled compensation mode. In contrast, the other mode (μ_-) has a weaker damping rate than either the atmosphere or ocean and exhibits a collaboration structure and therefore will be called the coupled collaboration mode

$$\mu_{\text{COLL}} \equiv \mu_- < \min(\mu_A, \mu_O) \quad \text{and} \quad (6a)$$

$$C_{\text{COLL}} \equiv C_- = \frac{b_O}{\mu_A - \mu_-} = \frac{\mu_O - \mu_-}{b_d} > 0. \quad (6b)$$

The solution above shows that, in general, the compensation mode is a strongly damped mode, while the collaboration mode is a weakly damped mode. Physically, the collaboration mode is weakly damped because it is subject only to the weak damping of negative IR feedback on the atmosphere at TOA, as seen in the schematic figure of Fig. 3b. In contrast, the compensation mode is heavily damped because it is subject to strong negative air–sea feedback at the ocean–atmosphere interface, as seen in the schematic figure of Fig. 3c. This difference in damping rate is most clear in the realistic parameter regime, which exhibits a weak TOA feedback relative to the surface feedback $B \ll B_d, B_O$, or approximately $b \ll b_d, b_O$, where, for simplicity, we have assumed $K_A \sim K_O \sim K$. Now, the two modes are strongly coupled, approaching the limiting values of

$$\mu_{\text{COMP}} \rightarrow \mu_A + \mu_O, \quad C_{\text{COMP}} \rightarrow -1 \quad \text{and} \quad (7a)$$

$$\mu_{\text{COLL}} \rightarrow b/(1 + b_d/b_O) \rightarrow 0, \quad C_{\text{COLL}} \rightarrow b_O/b_d. \quad (7b)$$

The compensation mode is heavily damped and exhibits a perfect compensation, while the collaboration mode is virtually undamped. For the standard parameters [after Eqs. (1d) and (1f)], the damping rate square of the two modes can be solved in Eq. (4) as $\mu_{\text{COLL}} = 0.24$ and $\mu_{\text{COMP}} = 5.89$. So, the damping rate is then $\sqrt{5.89/0.24} \approx 5$ times larger in the compensation mode than the collaboration mode, consistent with the scaling estimation in the realistic parameter regime in Eqs. (7a) and (7b).

The very weak damping of the collaboration mode implies that the remote climate response tends to be dominated by the collaboration response, rather than the compensation response, regardless of the initial generation mechanism. Physically, this collaboration response can be associated with, for example, the coupled response of the atmospheric Hadley circulation and the upper-ocean wind-driven subtropical cell (Held 2001; Vallis and Farneti 2009; Green and Marshall 2017). The dominance of the collaboration response in the remote region can be demonstrated in two examples in our EBM.

Figures 4a–d show an example of climate response to a reduction in TOA IR parameter B in the SH high latitudes [$x/(\pi/2) < -0.5$; Fig. 4e]. In the direct forcing region (gray shading), the reduced heat loss through TOA traps anomalous heat in the coupled system as seen in the energy budget (red dashed, Fig. 4d), warming both the atmosphere and ocean (red and blue solid lines, respectively; Fig. 4a), generating northward heat transports in both the atmosphere and ocean (red and blue solid, Fig. 4b) and, in turn, a forced collaboration

Collaboration Response to B

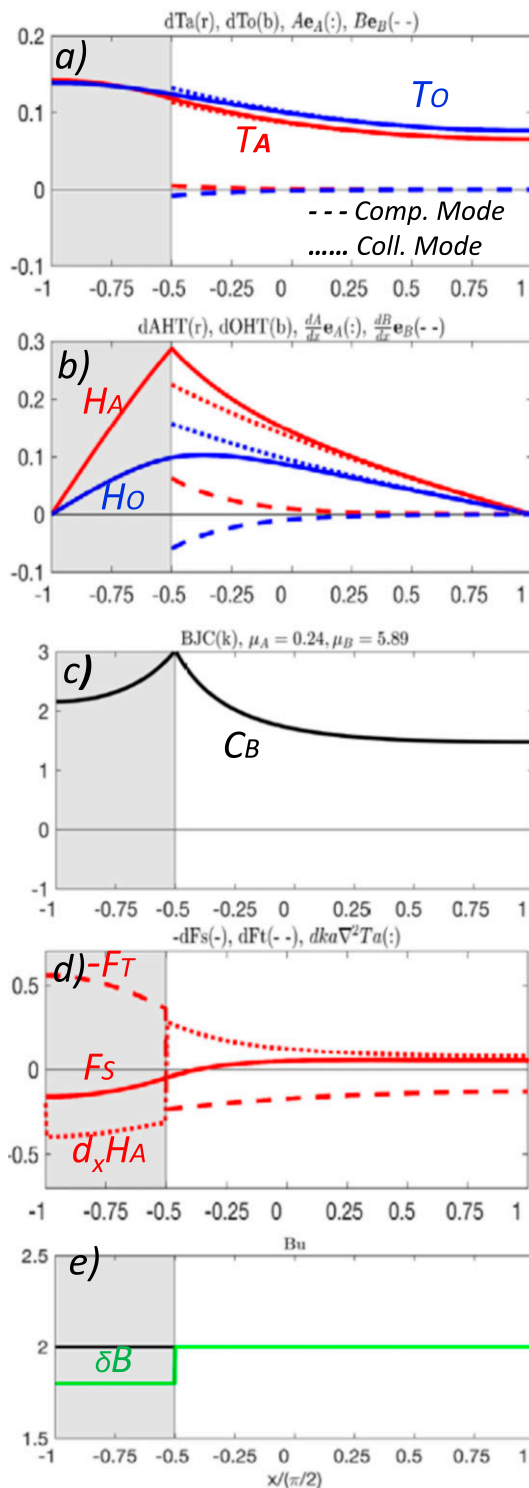


FIG. 4. As in Fig. 2, but for the heat transport response forced by a decrease of TOA IR feedback B south of $x/(\pi/2) < -0.5$ shown in (e). Inside the gray shaded region, the response is forced by the perturbation forcing; outside the shaded region, the response is

response as seen in the BJC ratio (Fig. 4c), which is consistent with the BJC ratio C_B derived in Eq. (3d). Away from the forcing region, the temperature anomaly decays slowly northward (red and blue solid, Fig. 4a) and is always dominated by a northward AHT and OHT (red and blue solid lines, respectively; Fig. 4b) as a collaboration response, as seen in the BJC ratio (Fig. 4c). Two reasons cause this remote collaboration response outside the forcing region. First, the forced response projects predominantly onto the collaboration mode at the edge of the forcing region $x/(\pi/2) = -0.5$. Second, the collaboration mode decays slowly northward during its propagation. To see the contribution of each mode explicitly, we project the total responses at each latitude onto the two eigenmodes. The eigenfunction structures of the two modes can be derived from Eqs. (6a) and (6b) under the boundary conditions of no fluxes at both poles. The total responses of temperatures (solid lines in Fig. 4a) and heat transports (solid lines in Fig. 4b) are then projected onto the two modes in the unforced region at each point such that the total response is the linear sum of the projections onto the two modes. The initial projection at $x/(\pi/2) = -0.5$ is predominantly on the collaboration mode (dotted) therefore, because of the dominant collaboration response in the forcing region there. Furthermore, the collaboration mode (dotted) decays much more slowly than the compensation mode (dashed) during its propagation northward. Indeed, for the standard parameters here, the damping rate is 5 times larger in the compensation mode than in the collaboration mode. As such, eventually, the far-field response is dominated almost completely by the collaboration mode, as seen in both the temperature (Fig. 4a) and heat transport (Fig. 4b). This leads to a BJC ratio of the total response always as a collaboration response away from the forcing region (Fig. 4c).

Figure 5 shows a more interesting example in which the remote climate response is initially a compensation response but is later reversed to a collaboration response in the far field. Now, the forcing is induced by the parameter B_d with a reduction in the SH high latitudes [$x/(\pi/2) < -0.5$; Fig. 5e]. In the forcing region, this reduces the downward heat loss from the atmosphere to the ocean in the energy budget (red dashed, Fig. 5d),

←

caused by the free propagation of the coupled modes originating from the edge of the forcing region $x/(\pi/2) = -0.5$. The projection onto the collaboration and compensation modes are plotted with dotted and dashed lines, respectively, for temperature in (a) and heat transport in (b). The full solution satisfies the no-flux boundary condition at $x = -\pi/2$ and $\pi/2$.

Compensation Response to B_d

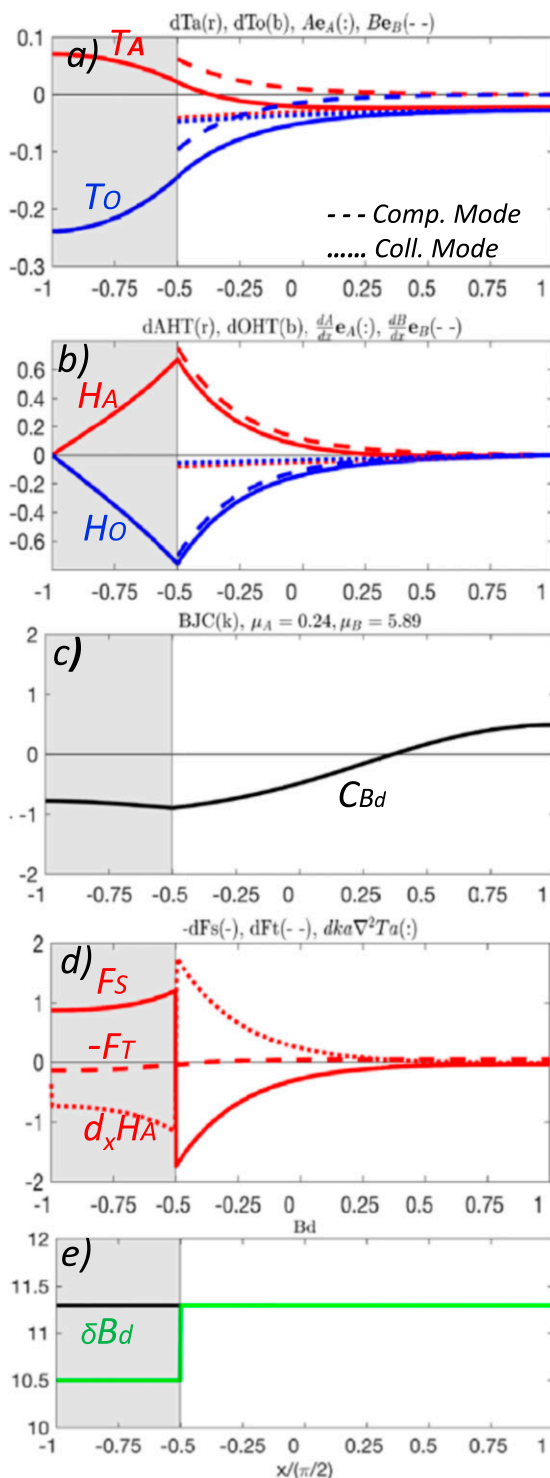


FIG. 5. As in Fig. 4, but for heat transport responses forced by a decrease of downward IR feedback B_d south of $x/(\pi/2) = -0.5$ as shown in (e).

warming the atmosphere (red solid) but cooling the ocean (blue solid) (Fig. 5a); this generates a northward AHT (red solid) but a southward OHT (blue solid) (Fig. 5b) and eventually a forced compensation response (Fig. 5c), consistent with the C_{B_d} in Eq. (3a). The total response, however, decays rapidly away from the forcing region such that in the NH extratropics [$x/(\pi/2) > 0.4$], the total response is reversed to a collaboration response (Fig. 5c), where the AHT and OHT, albeit weak, are both southward (red and blue solid, respectively; Fig. 5b). This change in the BJC ratio can also be understood in terms of the projections onto the two eigenmodes, as in Fig. 4. Now, the surface flux forces a dominant compensation response initially at $x/(\pi/2) = -0.5$, as seen in the much larger amplitude of the projection onto the compensation mode (dashed) than the collaboration mode (dotted) in both temperature (Fig. 5a) and heat transport (Fig. 5b) there. Northward, however, the compensation response decays rapidly, because the compensation mode decays 5 times faster than the collaboration mode. As such, the total response reverses to a collaboration response north of $x/(\pi/2) > 0.4$, as seen in the change in sign of the BJC ratio (Fig. 5c). Therefore, in spite of their different initial responses at $x/(\pi/2) = -0.5$, in both examples, the remote responses eventually become the collaboration response.

Our theoretical result here may offer an explanation of the robust remote collaboration response in the tropical–subtropical region across recent CGCM experiments in response to perturbation climate forcing at high latitudes (Deser et al. 2015; Hawcroft et al. 2016; Haywood et al. 2016; Kay et al. 2016; Green and Marshall 2017). In these experiments, the perturbation forcing does not cause significant change in the thermohaline circulation. As a result, the energy transport signal likely propagates mainly in the coupled collaboration mode and compensation mode. Since the compensation mode is strongly damped, the remote response is dominated by the collaboration mode as a collaboration response.

Our theory implies that active upper-ocean dynamic heat transport and, in turn, the coupled modes are essential for the remote collaboration response. The upper-ocean wind-driven dynamics is crucial for the damped compensation response in the remote region (Green and Marshall 2017). In a slab ocean without ocean dynamics (e.g., Kang et al. 2008; Green and Marshall 2017), the coupled model can generate a robust compensation response globally. One obvious reason is that in these experiments, the OHT forcing is prescribed across the globe and therefore can force an AHT response everywhere. The other reason, which is not very

obvious, is the small damping rate for the coupled mode. This can be seen in our coupled EBM, which becomes effectively a coupled atmosphere–slab ocean after setting $K_O = 0$ (similar to Liu et al. 2016). Now, one can show that the coupled system has a single mode of damping rate $\mu = b$, with the atmospheric temperature responding to the oceanic temperature anomaly as $T_A = B_O T_O / B_d$. In the realistic regime, $b \ll b_d$, this mode has a damping rate comparable with the collaboration mode in Eq. (7b) (but here there is no OHT because $K_O = 0$)—both have a damping rate much smaller than the atmospheric damping rate because $\mu = b < b + b_d \equiv \mu_A$. Therefore, in a coupled atmosphere–slab ocean model, the climate signal can propagate much farther away than in a fully coupled model. This remote response, however, has no contribution to the OHT (because $K_O = 0$) and in turn the BJC ratio. Therefore, the effective climate teleconnection of high-latitude climate forcing to the tropics as demonstrated in coupled atmosphere–slab ocean models can be caused either by the coupled propagation (Broccoli et al. 2006; Lu and Cai 2010) or a prescribed OHT forcing as a compensation response (Kang et al. 2008; Liu et al. 2016). In a fully coupled model with active ocean dynamics, as discussed regarding Figs. 2 and 3a, a compensation response can also be caused by the change of the thermohaline circulation (e.g., Zhang and Delworth 2005; Marshall et al. 2014; Green and Marshall 2017), but only if the thermohaline circulation is changed substantially. This is not the case in those CGCM simulations in the collaboration response (Deser et al. 2015; Hawcroft et al. 2016; Haywood et al. 2016; Kay et al. 2016; Green and Marshall 2017).

In summary, the remote response is determined mainly by the energy propagation in coupled modes and tends to be dominated by the weakly damped collaboration mode. If, however, the thermohaline circulation is perturbed significantly, then an effective teleconnection tunnel of OHT can still transport heat and, in turn, generate a remote compensation response.

5. Response to global warming

We now return to the forced response with a more “realistic” and complex forcing that consists of both surface and TOA fluxes. This is the case of global warming induced by an increased atmospheric concentration of CO_2 . Since global warming perturbs both the surface and TOA longwave fluxes, the final heat transport response depends on the competition between the surface and TOA forcing and, furthermore, the subtler balance with additional factors that are not considered in our EBM discussion above.

In response to global warming induced by the increased atmospheric concentration of CO_2 , most realistic climate models exhibit a compensation response, with an enhanced AHT but a reduced OHT (e.g., Hwang and Frierson 2010; Zelinka and Hartmann 2012; Feldl and Roe 2013; Roe et al. 2015). In our EBM, this corresponds to a poleward decreasing warming in the atmosphere and a polar amplification warming in the ocean. As proposed by Cai (2006), atmospheric heat transport can play an important role in this polar amplification response to global warming. It is proposed that, even in the absence of the positive feedback associated with high-latitude albedo, the atmosphere transports warm and moist air toward the high latitudes, where it increases the downward longwave radiation, heating the ocean and leading to a polar amplification. This global warming response can be studied in our coupled energy balance model using the radiative heat flux parameterization as in Cai (2006). As it turns out, in this case, the spatial variation of the feedback parameters is also critical. Therefore, we will start with the total energy budget equation before perturbation. Given an incoming solar radiation S , the total atmospheric and oceanic energy equations can be written as

$$0 = -2\varepsilon\sigma T_A^4 + \varepsilon\sigma T_O^4 + K_A d_{xx} T_A \quad \text{and} \quad (8a)$$

$$0 = -\sigma T_O^4 + \varepsilon\sigma T_A^4 + S(x) + K_O d_{xx} T_O. \quad (8b)$$

The climatological atmospheric and oceanic temperatures \bar{T}_A and \bar{T}_O , respectively, are determined by

$$0 = -2\bar{\varepsilon}\sigma \bar{T}_A^4 + \bar{\varepsilon}\sigma \bar{T}_O^4 + K_A d_{xx} \bar{T}_A \quad \text{and} \quad (9a)$$

$$0 = -\sigma \bar{T}_O^4 + \bar{\varepsilon}\sigma \bar{T}_A^4 + S(x) + K_O d_{xx} \bar{T}_O, \quad (9b)$$

where the mean atmosphere emissivity is $\bar{\varepsilon} \sim 0.8$. The solar radiation $S(x)$ decreases poleward and therefore forces mean temperatures $\bar{T}_A(x)$ and $\bar{T}_O(x)$ to decrease poleward (Figs. 6a, 7a). An increase in CO_2 concentration can be represented by an increased emissivity $\varepsilon' \sim 0.03$. The global warming response is therefore determined by linearized equations as follows:

$$0 = -\bar{\varepsilon}(B_d + B)T'_A + \bar{\varepsilon}B_O T'_O + K_A d_{xx} T'_A + \varepsilon'(I_O - I_A) - \varepsilon' I_A \quad \text{and} \quad (10a)$$

$$0 = -B_O T'_O + \bar{\varepsilon}B_d T'_A + K_O d_{xx} T'_O + \varepsilon' I_A. \quad (10b)$$

Here, the feedback sensitivity coefficients are denoted parallel to our Eqs. (1a) and (1b) as $B_d(x) = B(x) = 4\sigma \bar{T}_A^3(x)$ and $B_O(x) = 4\sigma \bar{T}_O^3(x)$. Note here that the negative feedback of turbulent heat flux is not included, to be consistent with Cai (2006). The perturbation IR forcing of global warming is proportional to the

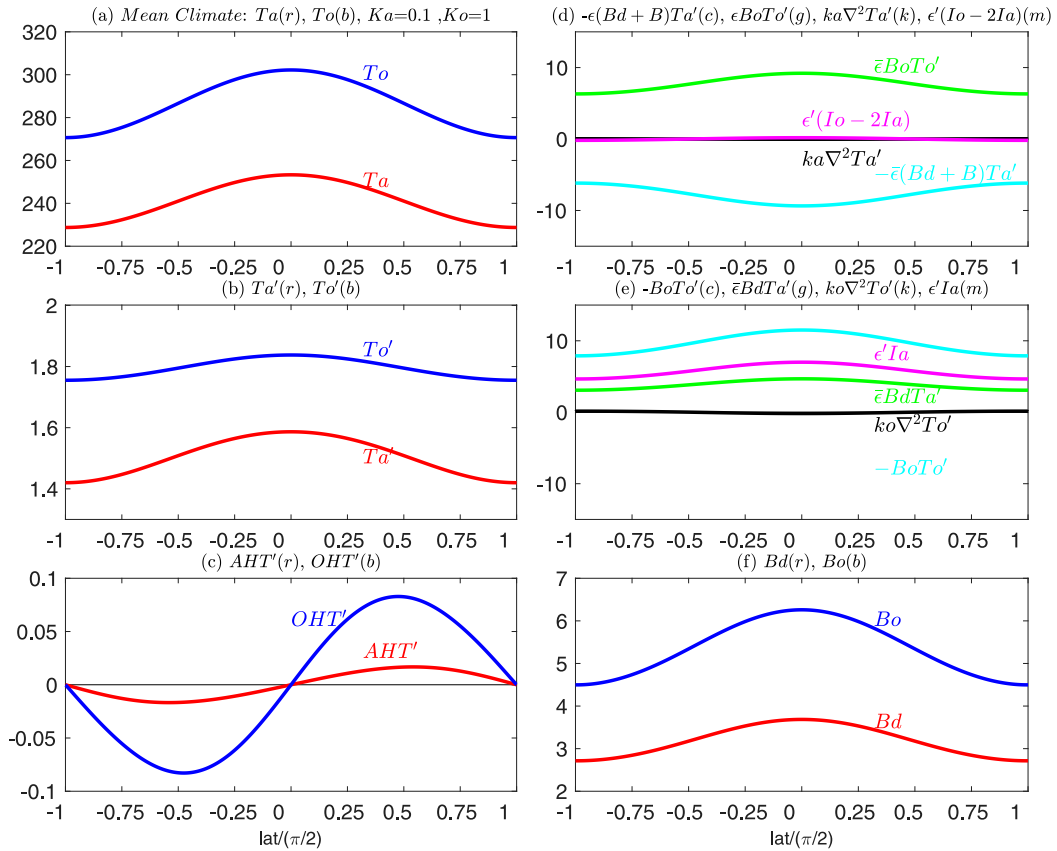


FIG. 6. Response to global warming in the case of a very weak AHT coefficient $K_A = 0.1$ in the coupled system [Eqs. (8a) and (8b)] in spherical coordinates with $K_O = 1$. (a) The mean atmospheric (red) and oceanic (blue) temperatures for the control experiment with $\varepsilon = 0.8$ as in Eqs. (9a) and (9b), with a solar radiation forcing that decreases poleward. The global warming responses to an increased emissivity of $\varepsilon' = 0.03$ (difference from the control) are shown for (b) temperatures (atmosphere, red; ocean, blue), (c) heat transports (AHT, red; OHT, blue), and (d) atmospheric and (e) oceanic energy budgets as in the linearized energy equations [Eqs. (10a) and (10b)]. (f) The spatial variation of the two feedback coefficients. In this case, both atmospheric and oceanic warming decrease poleward, accompanied by poleward AHT and OHT anomalies and, in turn, a collaboration response.

climatological IRs $I_A(x) = \sigma \bar{T}_A^4(x)$ and $I_O(x) = \sigma \bar{T}_O^4(x)$. Equations (10a) and (10b) show that the global warming response is forced by the competing effects between a surface forcing (downwelling IR $\varepsilon' I_A$), which contributes oppositely to the atmosphere and ocean, and a net heating forcing [atmospheric absorption $\varepsilon'(I_O - I_A)$], which only contributes to the atmosphere, and in turn the coupled system, here. From the physical mechanism related to the forced responses discussed in section 3, these two forcings tend to oppose each other (see the examples in Figs. 6d, 7d), with no obvious dominance of either forcing. Now, the heat transport response becomes dependent on other factors, notably the strength of AHT and the spatial variation of the feedback sensitivity parameters B_d , B , and B_O , as discussed below.

First of all, a large atmospheric heat transport K_A is crucial for producing the polar amplification in the surface T'_O . This is consistent with Cai (2006). This polar

amplification of T'_O , coupled with the poleward decreasing warming in the atmosphere T'_A , generates a compensation response with a poleward AHT anomaly and an equatorward OHT anomaly. The role of the AHT in this compensation response can be seen in two examples. For a small atmospheric diffusivity K_A (Fig. 6), the global warming response is close to the radiative equilibrium response, and the AHT almost vanishes (Fig. 6d). Since the global warming forcing, which is associated with $I_A(x)$ and $I_O(x)$, decreases poleward, temperature responses decrease poleward in both the atmosphere and ocean if the AHT is weak (Fig. 6b), corresponding to a collaboration response with the same poleward AHT and OHT (Fig. 6c). The downward atmospheric IR heats the ocean more on the equator ($\varepsilon' I_A$, purple in Fig. 6b), warming the ocean more on the equator (blue, Fig. 6b), which induces an upward IR feedback $-B_O T'_O$ (cyan in Fig. 6e) that is

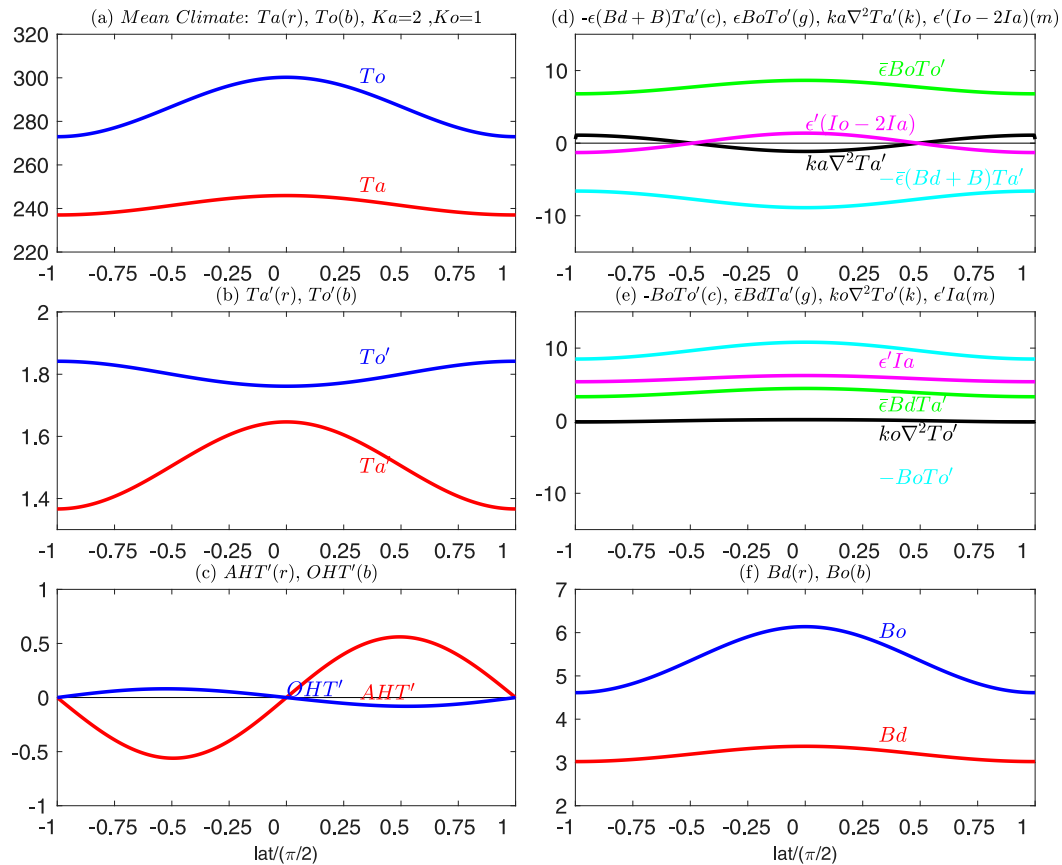


FIG. 7. As in Fig. 6, but for the case of a strong AHT coefficient $K_A = 1$. Now, ocean warming exhibits a polar amplification, corresponding to an equatorward OHT and, in turn, a compensation response.

absorbed by the atmosphere and heats the atmosphere more on the equator $\bar{\epsilon} B_O T'_O$ (green in Fig. 6d), leading to a stronger warming on the equator in the atmosphere, too (red, Fig. 6b). The direct upward radiative heating from the ocean to the atmosphere $\epsilon' I_O$, however, is almost balanced by its upward loss to space $-\epsilon' I_A$ and downward loss to the ocean $-\epsilon' I_A$ (purple in Fig. 6d). In this process, atmospheric heat transport is negligible (black in Fig. 6d), and the response is almost like a radiative equilibrium response. With a significant increase in K_A (Fig. 7), however, AHT becomes comparable with the radiative forcing $K_A d_{xx} T'_A$, (black in Fig. 7d), and the temperature response deviates significantly from the radiative equilibrium response. While the atmospheric warms and, in turn, AHT response still decreases poleward, ocean temperature exhibits a polar amplification, leading to an equatorward OHT (Figs. 7b,c), and in turn a compensation response. This surface polar amplification has been interpreted by Cai (2006) as being caused by a dynamic amplifier effect: an increased AHT poleward leads to a downward IR warming of surface temperature at high latitude, imposing an additional IR

heating on the surface that is independent of surface albedo feedback.

Here, we further point out that this downward IR forcing mechanism alone is insufficient to produce the polar amplification of T'_O and, in turn, the compensation response, at least in our EBM framework. Indeed, one can prove analytically that the global warming response always enhances both AHT and OHT poleward in the model, as long as all three feedback coefficients— $B_d(x)$, $B(x)$, and $B_O(x)$ —are spatially uniform. This can be understood physically as follows. First, regardless of K_A , the downward IR $\epsilon' I_A = \epsilon' \sigma \bar{T}_A^4(x)$ always decreases poleward (Figs. 6e, 7e) because of the poleward decreasing atmospheric climatological temperature \bar{T}_A (Figs. 6a, 7a) that is forced by the poleward decreasing ocean temperature \bar{T}_O through the upwelling IR forcing $\epsilon' I_O = \epsilon' \sigma \bar{T}_O^4(x)$ [see Eq. (9a)] and, ultimately, by the solar radiation $S(x)$ [see Eq. (9b)]. Instead, Eq. (10b) shows that the spatial structure of the ocean temperature response T'_O also depends on two competing feedback terms—a polar amplification feedback $-B_O T'_O$ and a poleward decreasing feedback $B_d T'_A$ —for which

sensitivity $B_O = 4\sigma\bar{T}_O^3$ and $B_d = 4\sigma\bar{T}_A^3$ decrease poleward (Figs. 6f, 7f). An increase in K_A increases the atmospheric mixing effect, which also reduces the gradient of the climatological \bar{T}_A (from Fig. 6a to Fig. 7a) and, in turn, the sensitivity B_d (from Fig. 6f to Fig. 7f), with nevertheless no significant impact on the gradient of \bar{T}_O and B_O . Therefore, the polar amplification feedback $-B_O T'_O$ prevails. This can be seen in the ocean heat budget. The atmospheric downward IR is indeed increased in the case of large K_A compared with the case of small K_A such that its poleward decreasing gradient is reduced significantly ($\varepsilon'I_A$, purple from Fig. 6e to Fig. 7e), favoring polar amplification in the ocean. This is consistent with Cai (2006) that the large poleward AHT ($K_A d_{xx} T'_A$, black in Fig. 7d) transports heat toward the poles, which then generates additional downward IR to the ocean in the polar region. However, this downward IR heating is still slightly larger in the tropics than the extratropics and therefore it alone is insufficient to generate a polar amplification in the ocean. Instead, strong IR damping in the tropics ($-B_O T'_O$, cyan in Fig. 7e) plays also a significant role in damping the tropical warming and eventually generates the polar amplification in the ocean (blue in Fig. 7b). Here, the strong AHT also reduces the gradient of the mean atmospheric temperature (red, Fig. 7a), because the downward IR feedback parameter B_d exhibits little change with latitude (red, Fig. 7f). As a result, the poleward decreasing atmospheric warming does feedback strongly onto the ocean temperature ($\varepsilon B_d T'_A$, green in Fig. 7e). Otherwise, a larger B_d in the tropics than in the extratropics could increase the downward heating to the tropical ocean, against the polar amplification warming in the ocean.

The reversal of OHT, and in turn the compensation response, with the increased K_A can be seen more clearly in the change of AHT and OHT responses to the continuous increase of K_A at an SH latitude (Fig. 8). Two cases of $K_O = 0.1$ (dashed) and 1 (solid) are shown, and the results are the same. When K_A is smaller than ~ 0.8 , both AHT (red) and OHT (blue) are poleward (negative), corresponding to a collaboration response. As K_A increases, the poleward AHT increases monotonically, but at a rate less than the linear rate of K_A itself, because of the reduction of the poleward decreasing atmospheric gradient. In contrast, the poleward OHT anomaly decreases and eventually reverses the sign to equatorward (positive) when K_A exceeds ~ 0.8 , corresponding to a polar amplification and a compensation response.

A further factor in producing a compensation response could be the reduced AMOC. This may be represented crudely in our model [Eqs. (1a) and (1b) or

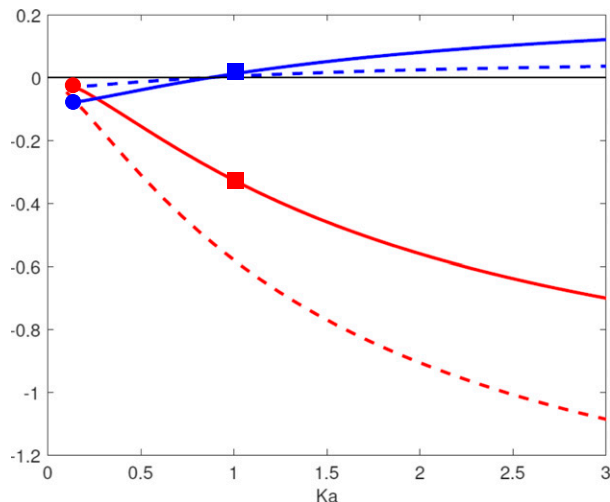


FIG. 8. AHT (red) and OHT (blue) responses to global warming at 70°S as a function of AHT efficiency K_A for two OHT efficiencies of $K_O = 1$ (solid) and 0.1 (dashed). It is seen that the AHT response is always an enhanced poleward AHT (negative) because of the greater warming in the tropics. The OHT response is also poleward for $K_A < 0.9$ (collaborative response) but then reverses to equatorward, and poleward warming for larger K_A (compensation response). The circle and squares correspond to the cases in Figs. 6 and 7, respectively.

Eqs. (3a) and (3b)] with a dependence of the oceanic diffusivity, which can be thought as proportional to the magnitude of the AMOC transport, to atmospheric emissivity as $K_O = \bar{K}_O(1 + m\varepsilon)$. Since AMOC tends to decrease in response to global warming (Meehl et al. 2007), this implies $m < 0$. One can see analytically that, even with constant feedback parameters B_d , B_O , and B , a modest rate of weakening of AMOC to global warming ($m < 0$) can generate a compensation response with an equatorward OHT anomaly and a poleward AHT anomaly (not shown).

In short, the global warming scenario represents a more complex case of mixed forcing perturbation in the surface and TOA fluxes, the variable feedback parameters with space, and the potential change of the AMOC. A strong atmospheric heat transport coefficient K_A affects both the perturbation and climatological temperatures significantly: the former induces a downward radiative forcing favorable for ocean temperature polar amplification, while the latter changes the feedback spatially such that it also favors polar amplification.

6. Summary and discussion

Using a coupled EBM, we addressed two questions on the heat transport responses: What is the coupled response of AHT and OHT to a general climate forcing, and what is the remote response of the coupled heat

transport to a local perturbation forcing? First, we show that the responses of AHT and OHT depend critically on the nature of the forcing. If the thermohaline circulation is not altered significantly, then a surface forcing, whether directly by radiation or indirectly by OHT or AHT convergence, tends to force a compensation response; in contrast, a net TOA radiative forcing tends to force a collaboration response. A change of the thermohaline circulation tends to produce a compensation response because it first induces an OHT change, which then forces the coupled system as an effective surface heat flux forcing. Second, the coupled system has two coupled energy transport modes: a compensation mode that is strongly damped by negative air–sea interaction and a collaboration mode that is only weakly damped by the TOA climate feedback. As such, the remote response tends to be dominated by the weakly damped collaboration mode. If, however, the thermohaline circulation is perturbed significantly, it can generate a remote compensation response through its deep ocean teleconnection tunnel of OHT.

Our model is highly idealized and many further studies are needed. Its idealized nature also limits its application to more complex models, or the real world. In particular, regarding the forced response, our theory shows a clearly different compensation response in response to surface and TOA forcing [Eqs. (3a)–(3d)]. But in more realistic cases or the real world, a perturbation forcing usually induces both the surface and TOA forcing. Therefore, the final response depends on the competition between the two types of forcing. When the two forcing effects are nearly balanced, the response becomes dependent on additional factors, such as the spatial variation of the feedback strength and forcing. This point has been seen in the example of global warming response in section 5. Therefore, without a detailed analysis of the induced perturbation forcing, our theory cannot explain the coupled heat transport responses in the global warming experiments in more complex models, such as those in Hwang and Frierson (2010) and Zelinka and Hartmann (2012).

In the meantime, some of our conclusions depend on more robust physical mechanisms. In particular, we believe that our conclusion on the remote response should be more robust. This is because the physical mechanisms behind the two coupled energy transport modes are simple and robust. Regardless of the details of the model, air–sea interaction is strongly negative, because of the strong turbulent heat flux sensitivity at the air–sea interface. In comparison, the negative feedback on TOA is weak because it is dominated by the longwave radiation at TOA. This difference of the feedback strength determines the damping nature of the two modes: the compensation mode involves strong

surface heat flux activity and therefore should be strongly damped, while the collaboration mode does not involve strong surface flux activity and therefore should be weakly damped by the TOA damping only. This suggests that our conclusion on the remote response should be applicable qualitatively to the coupled response in more complex climate models. This is confirmed in a preliminary test in a CGCM that exhibits a dominant remote collaboration response, when the thermohaline is not affected significantly (see the appendix). We speculate that our theoretical results may offer an explanation for the seemingly controversial results across CGCMs. With high-latitude perturbation, if the AMOC is altered significantly, then the climate response tends to exhibit a compensation response. This is consistent with many coupled model studies that show a compensation response induced by the change of AMOC (e.g., Vellinga and Wu 2008; Zhang and Delworth 2005; Zhang et al. 2010; Farneti and Vallis 2013) or a prescribed OHT forcing over the globe that can simulate the thermohaline forcing (e.g., Kang et al. 2008). Otherwise, the remote response is dominated by a collaboration response that is associated with the coupled atmosphere–upper ocean wind-driven circulation system when the AMOC is not perturbed significantly. This seems to be consistent with recent CGCM simulations of remote collaboration responses, when the AMOC is not perturbed significantly (Deser et al. 2015; Hawcroft et al. 2016; Haywood et al. 2016; Kay et al. 2016; Green and Marshall 2017).

Acknowledgments. We thank three anonymous reviewers for their constructive comments. This work is supported by Chinese Minister of Science and Education (MOSTSQ2017YFJC050038), Natural Science Foundation of China (NSFC41630527), National Science Foundation (NSF1656907), and Nanjing University of Information Science and Technology through a graduate fellowship. We thank Dr. M. Cai for the many discussions on the mechanism of global warming response.

APPENDIX

A CGCM Example of Remote Heat Transport Responses

As a preliminary test of our theory on the remote response, we analyzed perturbation simulations in a CGCM: the Fast Ocean Atmosphere Model (FOAM) (Jacob 1997). These experiments are originally designed to study the extratropical impact on tropical climate (Lu et al. 2017). The model design nature also allows us to examine the remote climate response of heat transports

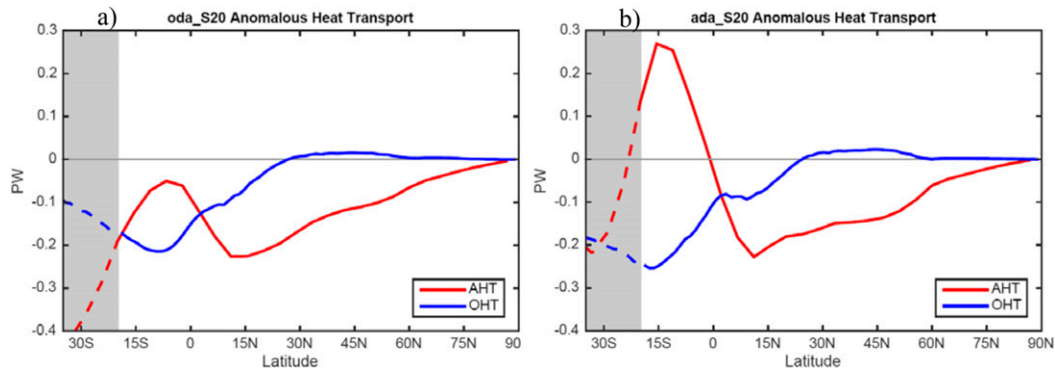


FIG. A1. AHT (red) and OHT (blue) responses in two CGCM (FOAM) simulations. The experiments are perturbed by forcing the model toward the observations using the ensemble coupled data assimilation method regionally south of 20°S . The AHT and OHT are calculated from the TOA and surface heat fluxes integrating from the North Pole. The response is derived as the ensemble mean difference between the perturbation experiment and the control experiment, which has no observations assimilated. (a) SST observations are assimilated. (b) Atmospheric temperature and wind observations are assimilated. It is seen that the initial collaboration response extends all the way to the tropics, while the initial compensation response is reversed to the collaboration response in the tropics.

here. We will discuss two sets of experiments. In the first set (Fig. A1a), present observations of SST from 1948 to 2015 are assimilated into the ocean model south of 20°S using a coupled ensemble filter. A climate response is derived as the difference from the control experiment in which no observation is assimilated. The forced response south of 20°S is artificial because data assimilation distorts energy conservation. Therefore, here, we will examine only the remote response north of 20°S , which is energetically consistent in the coupled system. At the boundary of the forcing region of 20°S , both the AHT and OHT anomalies are negative. This collaboration response is then seen to propagate northward into the tropics. This is in contrast to the second case, which is forced by assimilating atmospheric temperature and winds, instead of SST, south of 20°S (Fig. A1b). Now, at $\sim 20^{\circ}\text{S}$, the response happens to exhibit a strong compensation response, with a positive AHT and a negative OHT. This compensation response, however, decays rapidly northward. The AHT response reverses southward into the deep tropics, leaving a collaboration response. Thus, despite the opposite responses initially at 20°S , both of the remote responses into the tropics are collaboration responses. Similar results have been produced in additional experiments, with the data assimilation boundary pushed back to, say, 28°S (not shown). This remote collaboration response in the tropics is consistent with our theory of the propagation of the collaboration mode and the damping of the compensation mode. We note that the OHT becomes slightly positive north of 30°N in both cases, making the heat transports a slightly compensation response. This OHT signal may be related to a change of the model thermohaline

circulation that is found confined in the North Atlantic region. Furthermore, the collaboration response should be most robust in the tropic–subtropics, where the coupled Hadley circulation–subtropical cell provides a robust collaboration mechanism (Held 2001; Green and Marshall 2017).

REFERENCES

- Bjerknes, J., 1964: Atlantic air-sea interaction. *Advances in Geophysics*, Vol. 10, Academic Press, 1–82, [https://doi.org/10.1016/S0065-2687\(08\)60005-9](https://doi.org/10.1016/S0065-2687(08)60005-9).
- Broccoli, A. J., K. A. Dahl, and R. J. Stouffer, 2006: Response of the ITCZ to Northern Hemisphere cooling. *Geophys. Res. Lett.*, **33**, L01702, <https://doi.org/10.1029/2005GL024546>.
- Cai, M., 2006: Dynamical greenhouse-plus feedback and polar warming amplification. Part I: A dry radiative-transportive climate model. *Climate Dyn.*, **26**, 661–675, <https://doi.org/10.1007/s00382-005-0104-6>.
- Deser, C., R. A. Tomas, and L. Sun, 2015: The role of ocean–atmosphere coupling in the zonal mean atmospheric response to Arctic sea ice loss. *J. Climate*, **28**, 2168–2186, <https://doi.org/10.1175/JCLI-D-14-00325.1>.
- Farneti, R., and G. Vallis, 2013: Meridional energy transport in the coupled atmosphere–ocean system: Compensation and partitioning. *J. Climate*, **26**, 7151–7166, <https://doi.org/10.1175/JCLI-D-12-00133.1>.
- Feldl, N., and G. H. Roe, 2013: The nonlinear and nonlocal nature of climate feedbacks. *J. Climate*, **26**, 8289–8304, <https://doi.org/10.1175/JCLI-D-12-00631.1>.
- Green, B., and J. Marshall, 2017: Coupling of trade winds with ocean circulation damps ITCZ shifts. *J. Climate*, **30**, 4395–4411, <https://doi.org/10.1175/JCLI-D-16-0818.1>.
- Hawcroft, H., J. Haywood, M. Collins, A. Jones, A. C. Jones, and G. Stephens, 2016: Southern Ocean albedo, interhemispheric energy transports and the double ITCZ: Global impacts of biases in a coupled model. *Climate Dyn.*, **48**, 2279–2295, <https://doi.org/10.1007/s00382-016-3205-5>.

- Haywood, J., and Coauthors, 2016: The impact of equilibrium hemispheric albedos on tropical performance in the HadGEM2-ES coupled climate model. *Geophys. Res. Lett.*, **43**, 395–403, <https://doi.org/10.1002/2015GL066903>.
- Held, I. M., 2001: The partitioning of the poleward energy transport between the tropical ocean and atmosphere. *J. Atmos. Sci.*, **58**, 943–948, [https://doi.org/10.1175/1520-0469\(2001\)058<0943:TPOTPE>2.0.CO;2](https://doi.org/10.1175/1520-0469(2001)058<0943:TPOTPE>2.0.CO;2).
- , and B. Soden, 2006: Robust responses of the hydrological cycle to global warming. *J. Climate*, **19**, 5686–5699, <https://doi.org/10.1175/JCLI3990.1>.
- Hwang, Y.-T., and D. M. W. Frierson, 2010: Increasing atmospheric poleward energy transport with global warming. *Geophys. Res. Lett.*, **37**, L24807, <https://doi.org/10.1029/2010GL045440>.
- Jacob, R., 1997: Low frequency variability in a simulated atmosphere ocean system. Ph.D thesis, University of Wisconsin-Madison, 159 pp.
- Kang, S. M., I. M. Held, D. M. W. Frierson, and M. Zhao, 2008: The response of the ITCZ to extratropical thermal forcing: Idealized slab-ocean experiments with a GCM. *J. Climate*, **21**, 3521–3532, <https://doi.org/10.1175/2007JCLI2146.1>.
- Kay, J., C. Wall, V. Yettella, B. Medeiros, C. Hannay, P. Caldwell, and C. Bitz, 2016: Global climate impacts of fixing the Southern Ocean shortwave radiation bias in the Community Earth System Model (CESM). *J. Climate*, **29**, 4617–4636, <https://doi.org/10.1175/JCLI-D-15-0358.1>.
- Liu, Z., H. Yang, C. He, and Y. Zhao, 2016: A theory for Bjerknes compensation: The role of climate feedback. *J. Climate*, **29**, 191–208, <https://doi.org/10.1175/JCLI-D-15-0227.1>.
- Longworth, H., J. Marotzke, and T. F. Stocker, 2005: Ocean gyres and abrupt change in the thermohaline circulation: A conceptual analysis. *J. Climate*, **18**, 2403–2416, <https://doi.org/10.1175/JCLI3397.1>.
- Lu, F., Z. Liu, S. Zhang, and R. Jacob, 2017: Assessing extratropical impact on tropical bias in climate model using regional coupled data assimilation. *Geophys. Res. Lett.*, **44**, 3384–3392, <https://doi.org/10.1002/2017GL072890>.
- Lu, J., and M. Cai, 2010: Quantifying contributions to polar warming amplification in an idealized coupled general circulation model. *Climate Dyn.*, **34**, 669–687, <https://doi.org/10.1007/s00382-009-0673-x>.
- Marshall, J., A. Donohoe, D. Ferreira, and D. McGee, 2014: The ocean's role in setting the mean position of Inter-Tropical Convergence Zone. *Climate Dyn.*, **42**, 1967–1979, <https://doi.org/10.1007/s00382-013-1767-z>.
- Meehl, G. A., and Coauthors, 2007: Global climate projections. *Climate Change 2007: The Physical Science Basis*, S. Solomon et al., Eds., Cambridge University Press, 747–845.
- North, G. R., 1975: Theory of energy-balance climate models. *J. Atmos. Sci.*, **32**, 2033–2043, [https://doi.org/10.1175/1520-0469\(1975\)032<2033:TOEBCM>2.0.CO;2](https://doi.org/10.1175/1520-0469(1975)032<2033:TOEBCM>2.0.CO;2).
- Roe, G. H., N. Feldl, K. C. Armour, Y.-T. Hwang, and D. M. Frierson, 2015: The remote impacts of climate feedbacks on regional climate predictability. *Nat. Geosci.*, **8**, 135–139, <https://doi.org/10.1038/ngeo2346>.
- Rose, B. E., and J. Marshall, 2009: Ocean heat transport, sea ice, and multiple climate states insights from energy balance models. *J. Climate*, **66**, 2828–2843, <https://doi.org/10.1175/2009JAS3039.1>.
- , and D. Ferreira, 2013: Ocean heat transport and water vapor greenhouse in a warm equable climate: A new look at the low gradient paradox. *J. Climate*, **26**, 2117–2136, <https://doi.org/10.1175/JCLI-D-11-00547.1>.
- Shell, K. M., and R. C. Somerville, 2005: A generalized energy balance climate model with parameterized dynamics and diabatic heating. *J. Climate*, **18**, 1753–1772, <https://doi.org/10.1175/JCLI3373.1>.
- Stommel, H., 1961: Thermohaline convection with two stable regimes of flow. *Tellus*, **13**, 2, 224–230, <https://doi.org/10.1111/j.2153-3490.1961.tb00079.x>.
- Stone, P., 1978a: Constraints on dynamical transports of energy on a spherical planet. *Dyn. Atmos. Oceans*, **2**, 123–139, [https://doi.org/10.1016/0377-0265\(78\)90006-4](https://doi.org/10.1016/0377-0265(78)90006-4).
- , 1978b: Baroclinic adjustment. *J. Atmos. Sci.*, **35**, 561–571, [https://doi.org/10.1175/1520-0469\(1978\)035<0561:BA>2.0.CO;2](https://doi.org/10.1175/1520-0469(1978)035<0561:BA>2.0.CO;2).
- Trenberth, K., and J. M. Caron, 2001: Estimates of meridional atmosphere and ocean heat transports. *J. Climate*, **14**, 3433–3443, [https://doi.org/10.1175/1520-0442\(2001\)014<3433:EOMAAO>2.0.CO;2](https://doi.org/10.1175/1520-0442(2001)014<3433:EOMAAO>2.0.CO;2).
- Vallis, G., and R. Farneti, 2009: Meridional energy transport in the coupled atmosphere–ocean system: Scaling and numerical experiments. *Quart. J. Roy. Meteor. Soc.*, **135**, 1643–1660, <https://doi.org/10.1002/qj.498>.
- Vellinga, M., and P. Wu, 2008: Relationship between northward ocean and atmosphere energy transports in a coupled climate model. *J. Climate*, **21**, 561–575, <https://doi.org/10.1175/2007JCLI1754.1>.
- Wunsch, C., 2005: The total meridional heat flux and its oceanic and atmospheric partition. *J. Climate*, **18**, 4374–4380, <https://doi.org/10.1175/JCLI3539.1>.
- Yang, H., Y. Zhao, and Z. Liu, 2016: Understanding Bjerknes compensation in atmosphere and ocean heat transports using a coupled box model. *J. Climate*, **29**, 2145–2160, <https://doi.org/10.1175/JCLI-D-15-0281.1>.
- Zelinka, M. D., and D. L. Hartmann, 2012: Climate feedbacks and their implications for poleward energy flux changes in a warming climate. *J. Climate*, **25**, 608–624, <https://doi.org/10.1175/JCLI-D-11-00096.1>.
- Zhang, R., and T. Delworth, 2005: Simulated tropical response to a substantial weakening of the Atlantic thermohaline circulation. *J. Climate*, **18**, 1853–1860, <https://doi.org/10.1175/JCLI3460.1>.
- , S. M. Kang, and I. M. Held, 2010: Sensitivity of climate change induced by weakening of the Atlantic meridional overturning circulation to cloud feedback. *J. Climate*, **23**, 378–389, <https://doi.org/10.1175/2009JCLI3118.1>.